The Structural Pathway from its Solvated Molecular State to the Solution Crystallisation of the α- and β-Polymorphic Forms of Para Amino Benzoic Acid

Ian Rosbottom [a,#], Thomas D Turner [a,&], Cai Y Ma [a], Robert B Hammond [a] and Kevin J Roberts [a,]*

[a] Centre for the Digital Design of Drug Products, School of Chemical and Process Engineering, University of Leeds, Woodhouse Lane, Leeds, LS2 9JT, UK

Chin W Yong [b,c], Ilian T Todorov [b]

[b] Scientific Computing Department, Science and Technology Facilities Council, Daresbury Laboratory, Warrington, WA4 4AD, UK

[c] Division of Pharmacy and Optometry, University of Manchester, Manchester, UK

Current addresses:

[#] GlaxoSmithKline, Gunnels Wood Rd, Stevenage, SG1 2NY, UK

[&] School of Mechanical Engineering, University of Leeds, Leeds, LS2 9JT, UK

* Corresponding Author

Table of Contents (for review purposes only)

Abstract

Para amino benzoic acid (PABA) has two well-characterised α- and β-polymorphic forms and, whilst both crystallise in the monoclinic space group P2$_1$/n, they have quite different crystal chemistry and crystallisability behaviour. Previous work has shown that the molecular conformation deformation energy in the crystalline state is higher for the β-form than for the α-form and that the lattice energy for the former converges more slowly than for the latter overall. This suggests that not only is there a higher barrier to crystallisation for the β-form but also that low solution supersaturations might be needed for it to preferentially nucleate. Additionally, solute cluster propensity and solute solvation energetic analysis highlights the importance of an aqueous solvation environment in inhibiting the α-form's strong OH…O carboxylic acid hydrogen bond (H-bond) dimer. Despite this, the detailed molecular-scale pathway from solvated molecules to 3D crystallographic structure still remains unclear, most notably regarding how the nucleation process is activated and how, as a result, this mediates the preferential formation of either of the two polymorphic forms.

Molecular dynamics (MD) simulations coupled with FTIR studies and intermolecular synthon analysis addresses this issue through characterisation of the propensity of the incipient bulk synthons that are important in the crystallisation of the two polymorphic forms within the solution state. MD molecular trajectory analysis within crystallisation solutions reveals a greater propensity for OH…O synthons (both single H-bonds and homodimers) typical of the α-form and NH…O synthons found in both the α- and β-

forms when compared to aqueous solution but much lower propensities for the β-form's "fingerprinting" OH…N and π-π stacking synthons. In contrast, data from the aqueous solution environment reveals a much greater propensity for the β-form's π-π interaction synthons.

IR dilution studies in acetonitrile in the carbonyl region reveal the presence of two C=O vibrational stretching bands, whose relative intensities vary as a function of solution dilution. These were assigned to the solvated PABA monomer and a COOH dimer of PABA. Similar data in ethanol shows a main C=O stretching band with a shoulder peak suggesting a similar monomer vs dimer speciation may exist in this solvent. The IR data is consistent with the organic solvent MD data, albeit the corresponding analysis for the aqueous solution was precluded due to the latter's strong OH vibrational mode which restricted validation in aqueous solutions.

Keywords: Para amino benzoic acid (PABA); Lattice Energy; Solute Solvation Energy; Molecular Conformational Deformation Energy; Molecular Dynamics; FTIR Spectroscopy; Hydrogen Bonding; Solubility; Metastability; Nucleation Kinetics

List of Symbols and Abbreviations

AcN:	Acetonitrile
ATR:	Attenuated total reflectance
Aα, Aβ:	Synthon A of α-form, synthon A of β-form
DFT:	Density functional theory
EtOH:	Ethanol
FTIR:	Fourier-transform infrared spectroscopy
H2H:	Head-to-head
H2T:	Head-to-tail
H-bond:	Hydrogen bond
IR:	Infra-red
MD:	Molecular Dynamics
PABA:	Para amino benzoic acid
q:	Solution cooling rate (m/s)
Q:	Scattering vector (nm^{-1})
SAXS:	Small angle X-ray scattering
Tc:	Crystallisation on-set point (critical temperature) (^{o}C)
vdW:	van der Waals
ΔH_{diss}:	Enthalpy of dissolution (kcal/mol)
υ:	IR spectrum wavenumber (cm^{-1})

1. Introduction

In solution crystallisation processes, understanding and controlling the transition pathway associated with the assembly of molecules from their supersaturation solvated state into different polymorphic crystalline solids, represents a significant grand challenge for the physical-chemical sciences [1].

Industrial utilisation of crystalline high-value materials is highly desirable, particularly so within the pharmaceutical and fine chemical industry, reflecting e.g. the high material purity enabled through the crystallisation process. To produce material in the crystalline state with the required yield and without compromising its stability, solution crystallisation still provided one of the most reliable and sustainable methods for manufacture. However, many organic materials display polymorphism, where such different crystal structures can have very different physico-chemical properties such as bioavailability, stability and morphology. However, crystallisation into the correct form is of vital importance when developing an effective and sustainable manufacturing process.

It has been hypothesised that the degree to which crystallisation conditions, such as solvent, temperature and concentration, can encourage the formation of intermolecular solute structuring in solution which can, in turn, influence crystallisation behavior and, through this, result in different polymorphic form of the material. Knowledge of solution structural behavior as a key part of the crystallisation design process could allow for a much more targeted process development which could, in principle, greatly

reduce the cost and time needed.

Characterisation of the solid-state intermolecular interactions present in organic crystal structures has resulted in a good understanding of the crystal chemistry of these materials. Indeed, it has become possible to use molecular modelling to predict the physical properties of molecular crystals, such as their polymorphic stability [2, 3], thermal expansion [4], morphology and surface chemistry [5, 6], habit modification [7, 8], surface wettability [9] and API/excipient compatibility [10-12]. In contrast, predicting the intermolecular chemistry of the solution phase can be much more demanding and one requires more sophisticated computational design tools, such as afforded by the application of molecular dynamics (MD) simulation. In this, extracting the details of the intermolecular interactions from successful MD simulations is far from straightforward, often relies on qualitative estimations from limited snapshots of the simulations.

Recent work by Yong et al [13-15] has demonstrated a new and more efficient approach when setting up MD simulations notably by providing more flexibility of the user interface, e.g., in interatomic forcefield selection and atom typing. The new approach also allows for more rational MD data analysis, notably in terms of searching for correlations between the relative positions of atoms within selected target molecules of interest through the use of distance and angular criteria to monitor the propensity of non-bonded intermolecular contacts.

This approach has been used to interrogate and characterise the propensity of incipient bulk synthons within the simulated solution-state through targeted analysis of the MD trajectory files. Through this holistic approach, intermolecular interactions between the solvated benzoic acid molecules present within hexane solutions were cross-correlated with the strongest intermolecular interactions found in the crystal structure of this material through studies which also revealed self-consistency with solution infra-red (IR) spectroscopy data [15, 16].

The above approach is extended through this work to examine the solution/solid-state pathways associated with para amino benzoic acid crystallisation and with the specific aim to characterise the role played by solvent choice (ethanol, acetonitrile and water) in terms of mediating and controlling the resulting polymorphic form of the materials as identified through synthon analysis of the α- and β-polymorphic forms in the solid state. These MD simulations are coupled with experimental solution-state IR spectroscopy studies for model validation.

2. Para Amino Benzoic Acid

This section provides a selective review of some key research related to the solution crystallisation of para amino benzoic acid (PABA). A much longer version of Section 2 is provided in Supplementary Information.

2.1 Molecular Properties and Crystallographic Structures

Para-aminobenzoic acid (PABA), an organic compound, also known as vitamin B10, is a white crystalline substance with molecular formula $(NH_2)(C_6H_4)(COOH)$, consisting

of three molecular moieties: an aromatic benzene ring substituted with carboxylic acid and amino groups which are para with respect to each other (**Figure 1**).
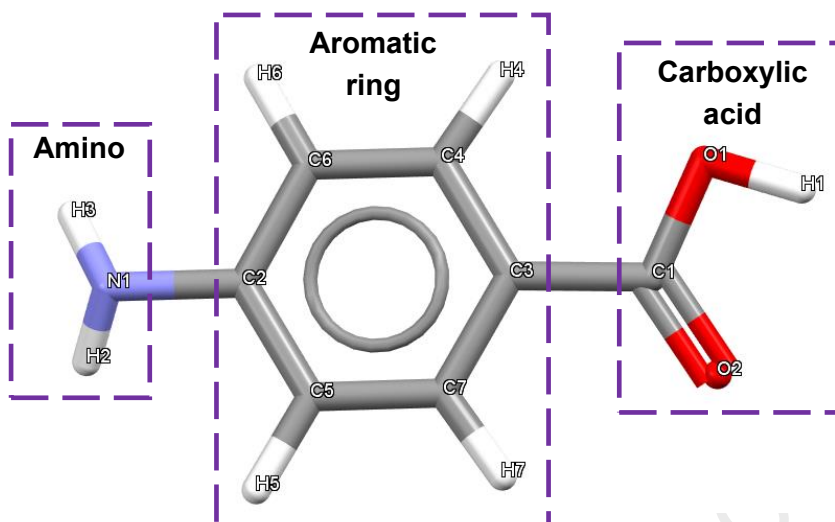
Figure 1. The molecular structure of para-aminobenzoic acid with the atom notations and the three molecular moieties (functional groups): aromatic ring, carboxylic acid and amino group as indicated in the boxes.

The crystal structures of the α- and β-forms of para-aminobenzoic acid are discussed in **Section S1.1**, Supplementary Information. Characteristic molecular descriptors and associated crystallographic structural data for PABA is summarised in **Table S1**. Interestingly, the β-form is more close packed with a higher density and less void space than the α-form albeit its melting point is lower than the α-form [17]. Analysis of the hydrogen bonds (H-bonds), as shown in **Table S2**, reveals that they are stronger in the β-form structure than in the α-form, as evidenced by the shorter H-bond lengths in the β-form than in the α-form. The molecular descriptors for PABA (**Table S1**) are compared with the representative pharmaceutical materials [3, 18] in **Section S1.1**.

2.2 Crystal Chemistry and Intermolecular Interactions

The examinations of solid-state chemistry of α- and β-form crystal structures [19] found that the α-form has strong H-bonding carboxylic acid OH…O dimer interactions, π-π stacking and NH…O interactions (**Figure 2(a)**) and that it crystallises with a needle- or lath-like morphology at higher temperatures. In contrast, the β-form has a characteristic 4-membered H-bonding ring comprising identical pairs of alternating OH…N and NH…O interactions and crystallises with a prismatic equant morphology (**Figure 2(b)**).
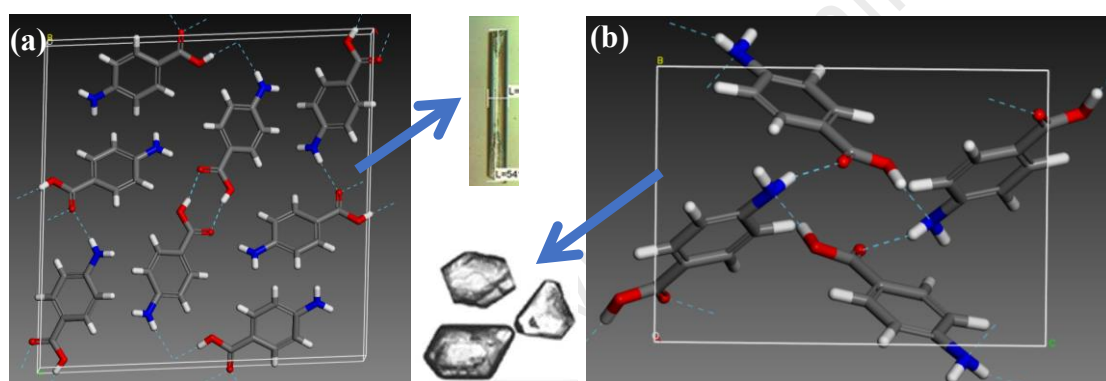
Figure 2. The crystal packing structures of para-aminobenzoic acid: (a) α-form; (b) β-form with their H-bonding networks and also observed morphologies (data derived from [19]).

Detailed molecular conformational analysis for these two polymorphic structures reveals some interesting differences (**Figure S3**). The rigid planar COOH dimers formed in the α-form crystal structure strongly hold the COOH group planar (**Figure 2(a)**). The NH…O H-bond is also relatively planar, leading overall to the α-form's tetra-molecular core building block remaining planar. Therefore the carboxyl acid group was found to be very close to the planar conformational minima and also the slight pyramidal bend of amino group close to the pseudopyramidal conformational

minima (**Figure S3**). On the contrast, the 4-membered H-bond ring in β-form structure distorts conformation of both functional groups as the OH…N H-bond pulls N atom towards OH group and the NH…O H-bond pulls the H atom towards the C=O group (**Figure 2(b)**). Hence, the carboxyl acid group was found to be slightly rotated away from a planar conformation, whilst the amino group was found to be more pyramidal (**Figure S3**). This reflects the need to complete the β-form's tetra-molecular H-bonded ring structure. As the α-form PABA conformation is closer to the minimum energy conformation (**Figure S3**), this would present a lower energy barrier to the crystallization of α-form when compared to the β-form, consistent with the known challenges in crystallising the β-form. That said, whilst the conformation deformation penalty could imply lower crystallisability of the β-form, once formed the strength of its core 4 member H-bonding ring structure would suggest a strong and stable arrangement for its subsequent development and growth (**Table S2**).

2.3 Solution Properties, Solvation and Solubility

Synthon propensity studies [19, 20], using the COSMO-RS approach, was ultilised to compare the relative populations of the energetically top-ranked synthons (Aα, Bα and Aβ, Bβ) in solution for a range of solvent systems (**Figure S5**). Synthon Aα associated with OH…O H-bonding interactions was found to be dominant for all solvents studied with the exception of water where the concentration of this synthon was found to be much lower and where π-π interactions were much more prevalent notably the π-π head-to-head (H2H) (synthon Bα) and head-to-tail (H2T) (synthon Aβ) interactions

11

which were found to be the most stable. In this, calculation of the surface charge distributions for the synthons reveals that the π-π interaction synthons (Bα, Aβ) have greater polar surface area when compared to the OH…O H-bonding synthons (Aα, Bβ). Overall, whilst the data supports the preferential crystallisation of the α-form from most solvents (except water), it does suggest that the β-form would be more likely to be crystallised from aqueous solutions.

A more detailed analysis of the intermolecular chemistry associated with the solvation of PABA molecules has been provided using intermolecular grid-search methods [21-23] which reveals (**Figure S6**) the predicted solvation shell structures for 3 solvent systems, EtOH, AcN and water (further details can be found in **Section S1.3**, Supplementary Information). The solvation energies confirms PABA to be well-solvated by the protic solvent EtOH which can interact strongly with both the aromatic ring through van der Waals interactions with the alkyl group and with the carboxylate through H-bonding. In contrast, the aprotic AcN solvates to a much lesser degree only forming only quite limited interactions with the COOH group compared to EtOH and water. Water, in contrast, fails to solvate the whole surface area of the PABA molecule apart from COOH group, particularly the amino group and the hydrophobic phenyl ring. This would also be consistent with its much lower solubility.

Solubility data [24], obtained from solution dissolution measurements (**Figure S7(a-c)**), upper plots) was analysed using van't Hoff plots for EtOH, AcN and water solvents (**Figure 3(a)**). These reveal less than ideal solubility (activities -0.91, 0.43, 0.02,

respectively) for all three solvents, consistent with a solution structure with an enhanced degree of solute/solute interactions and associated solute clustering.

2.4 Metastability, Solute Clustering and Nucleation

Analysis of the slopes of the associated crystallisation on-set points (Tc) as a function of the solution cooling rate (q) probing the kinetic balance between the relative rates of supersaturation generation and nucleation, provides a helpful indication as to the relative crystallisabilities (**Figure S7(a-c)**, lower plots)) for the three solvents. The data shows distinctly different behavior between the 3 solvents with water having a much flatter slope compared to EtOH and AcN, respectively, suggesting the rate-limiting parameters regarding crystallisability would have an order of (kinetics driven) EtOH > AcN > water (thermodynamics driven). Also as shown in (**Figure 3(a)**), the crystallisation on-sets in EtOH as a function of cooling rate shows a marked difference in slope with respect to the ideal solubility line, moving away from the equilibrium solubility which is slightly less than ideal to greater than ideal with increasing cooling rate, undercooling and hence supersaturation. Hence, qualitatively taking the slope as an indicator of the enthalpy of dissolution (ΔH_{diss}), ΔH_{diss} decreases from ideal solubility (2500 J/mol) to 488 J/mol (1.0 °C/min) as the solutions undercool. This change in the apparent crystallisability with increased cooling rate can also be seen in the data when replotted in terms of critical supersaturation at Tc (**Figure 3(b)**). This reveals that the highest cooling rates access a much wider range of supersaturations and nucleation cluster sizes across the solute concentration range (1.2 – 1.6) when compared

13

to lowest cooling rates (1.05 – 1.10).
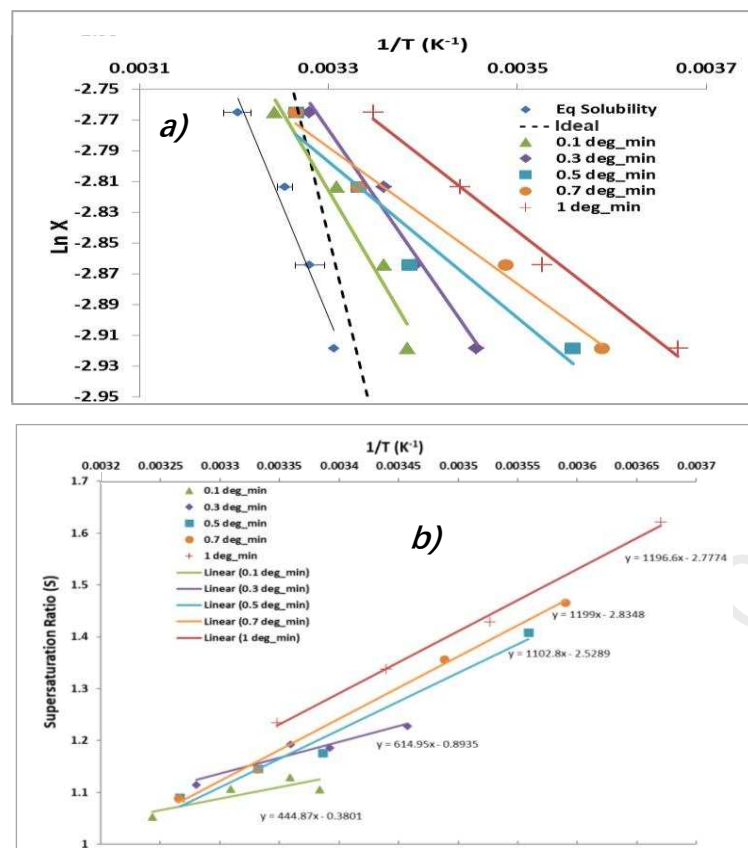
Figure 3. (a) Crystallisation temperatures of PABA in EtOH with van't Hoff coordinates, showing a marked differences in slope with respect to the ideal solubility line (---) and (b) supersaturation ratios in van't Hoff plotting (data derived from [24]).

Analysis of the polythermal crystallisation behavior as a function of solvent type and solution concentration indicated that the nucleation mechanism was mostly instantaneous and consistent with a two-step nucleation mechanism [24] except at low solute concentrations where it was progressive. Comparatively for the instantaneous cases, it could be said that EtOH was more instantaneous than AcN and water, this perhaps reflecting their relative solubilities [24].

The strong evidence for solute clustering from the less than ideal equilibrium

14

solubilities and instantaneous nucleation mechanism has been further examined using small angle X-ray scattering (SAXS) [25, 26]. The data confirmed the formation of solvent clusters within PABA in ethanolic solutions during cooling, highlighting at low Q an increase in cluster numbers and their size (> 40 nm) during cooling. Such clustering behavior is consistent with a number of previous studies on e.g. glycine [27], citric acid [28], and L-isoleucine [29]. Simultaneous analysis at high Q reveals solution de-supersaturation during cooling with evidence for formation of small cluster structures (ca. 1 - 2 nm) well matched to the overall dimensions of the Aα synthon.

A tentative nucleation pathway for PABA crystallisation from EtOH solutions is shown schematically in **Figure 4** which draws together the structural information obtained from the analysis of the modelling and experimental data to date. This indicates the progress of nano-scale assemblies from large disordered liquid-like PABA nano-clusters (dimers and monomers) in under-saturated condition, then the growth of these clusters in sizes under supersaturated conditions including the increasing degree of structural ordering at cluster/solution interface increasing the mass fractal dimension with their increasing interfacial smoothness and faceting at the interface and through to the formation of the crystalline phase (nuclei) by further growth. Overall, the data supports a two-step nucleation mechanism associated with the formation and development of nano-crystallite clusters together with the growth of smaller molecular clusters.
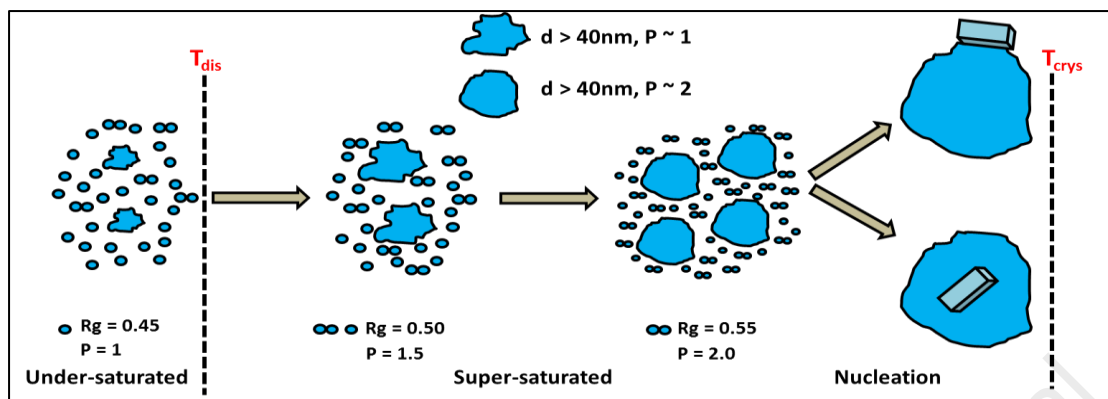
Figure 4. The tentative structural schematic of α-PABA nucleation pathway from EtOH solutions, based on the modelling and experimental evidence obtained so far, indicating large liquid-like clusters surrounded by a population of monomer and dimerised PABA molecules. Note the pathway for β-PABA nucleated in water can have different parameters. Rg is the radius of gyration which is related to cluster size (nm) and P is the fractal dimensionality and related to interface structure where a higher value infers a more ordered interface (data derived from [26]).

It is important to remark that the SAXS measurements require good contrast between the aggregated and continuum phases demanding, in turn, comparatively high solute concentrations. This aspect was linked SAXS studies to EtOH solutions (only) and in this case only at the relatively high solute concentration typified by instantaneous nucleation. In effect, this restriction precludes SAXS studies over a range of concentrations in EtOH and on the AcN and aqueous solutions. Hence, at this stage we do not know how this model would apply more generally.

3. Materials and Methods

3.1 Molecular Dynamics Simulations

Molecular modelling of intermolecular ordering in the solution state were performed using the integrated molecular dynamics (MD) software package developed by

16

Daresbury Laboratory, namely DL_FIELD (MD input files, atom type standardisation and forcefield selection) [13], DL_POLY (MD simulations) [30] and DL_ANALYSER (MD trajectory file analysis) [14] which all form part of the DL_Software system [31].

For this study, the Cartesian coordinates of a single molecule of PABA was inputted into DL_FIELD, where the concentration, forcefield and solvent was specified and the CONTROL, FIELD and CONFIG files needed for input into DL_POLY for MD simulations were constructed. The simulations were carried out using a 60 $Å^3$ periodic simulation box and with all intermolecular forces and their associated interaction energies being calculated using the Amber GAFF forcefield [32].

Three crystallising solution systems were examined: notably AcN (polar, aprotic), EtOH (polar, protic) and water (polar, protic) consistent with previous studies regarding solvation energies [23, 33], solvent-dependant synthon propensities [20] and nucleation kinetics [24, 25]. The simulations were carried out at a solute concentration of 0.1 g/ml and at a temperature of 20 °C which reflect the different PABA solubilities in these three solvents. This corresponded to solution supersaturations of ca. 1.2, 1.0 and 5.0 respectively.

To ensure effective equilibration, a constant energy simulation was run with constant scaling at 400 K for approximately 800 ps to remove any pre-existing solution chemistry from the solution box generation. The solution was then cooled to the sampling temperature of 293 K using a constant energy ensemble with constant scaling.

The scaling was removed and, if the temperature was observed to remain around the sampling temperature, then the solution was deemed acceptably equilibrated. The solution was then run for a short time using the Berendsen NVT ensemble [34], before being changed to the Berendsen NPT ensemble [34] until the box size no longer fluctuated. The sampling simulations were run for 10.0 ns each with a time step of 0.002 ps using the Nosé-Hoover NPT ensemble with thermostat and barostat relaxation times of 4.0 ps and 5.0 ps, respectively [35].

The standardised notation for the atom typing using the DANAI notation [14] within DL_FIELD was exploited for searching within the HISTORY trajectory files resulting from the MD simulations using DL_ANALYSER. Drawing upon the approach developed through previous work on benzoic acid [15], both the macro interactions that define the intermolecular interactions between functional groups of atoms as well as the micro interactions that define the exact atomic scale geometry of the selected interactions were characterised. The latter was based upon the key intermolecular synthons and their local inter-atomic geometry involved in the molecular assembly and crystallisation of the α- and β-forms of PABA [6]. Specifically, the trajectory files obtained from solution-state MD simulations were examined for the presence of the selected interacting groups, given in **Error! Reference source not found.**, in order to assess the extent to which the PABA molecules in their solution state undergo a degree of pre-ordering prior to crystallisation. In this analysis, any H-bonding interactions occurring at a distance of less than 2.5 Å and an interatomic angle of 120° or more in

angle were counted, whilst the close π-π parallel packing of the aromatic groups in PABA were only counted when they were closer than 4.5 Å and within a 20° angle or less.

Whilst the analysis here has focussed on the above important H-bonded and non-bonded interactions, the more subtle "finger printing" differences between the latter interactions between the α-form (H2H chains) and the β-form (H2T dimer pairs) were not probed. Overall, through this work, the extent to which the intermolecular synthons present in this pre-ordered solution state mirrors those present with the crystal structures following crystallisation was examined.
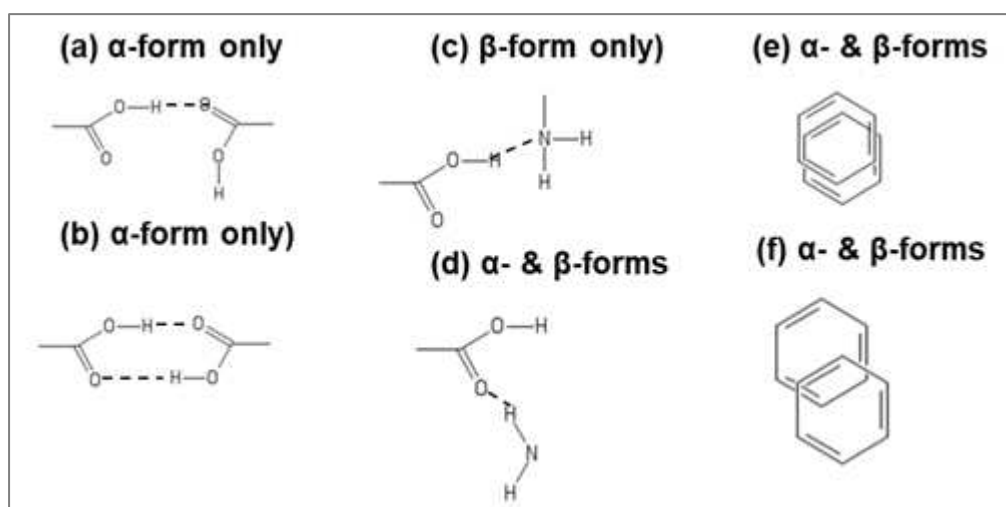
Figure 5. Molecular diagrams highlighting the intermolecular interactions searched in the solution-state MD trajectory files for PABA using DL_ANALYSER in relation to the known polymorphic forms: carboxylic to carboxylic interactions associated with single OH…O H-bonded (a) & double OH…O (b) (α-form only) carboxylate group H-bonding interactions; amino to carboxylic group interactions associated with (c) NH…O (α- & β-forms) & (d) OH…N (β-form only) H-bonding; inter-phenyl ring π-π interactions associated with both occluded (e) and staggered (f) structures.

3.2   IR Spectroscopy Experiments

PABA (99.9%) in its α-form was purchased from Sigma Aldrich and used as supplied and β-form PABA was obtained by slurry inter-conversion from the α-form at 5°C using a 500ml temperature-controlled jacketed crystallisation vessel. AcN (99%) was supplied by Alfa Aesar, EtOH (99.9%) by VWR and deionised water in-house.

Solution-state samples in EtOH and AcN were prepared using the α-form PABA dissolved in solvent in 10 ml screw top vials with magnetic stirring at 300 rpm which were left to equilibrate for 24 hours and passed through a 0.45 μm filter prior to use. The concentrations studied in EtOH were 147.7, 130, 110 and 80 g/kg, corresponding to saturation temperatures of 20, 3, -3 and -17°C, respectively. The saturation concentrations of samples in AcN were 64.4, 60 and 55 g/kg corresponding to saturation temperatures of 20, 18 and 15 °C.

The IR spectra of PABA in solid and in solution forms were collected using a Nicolet Nexus FTIR spectrometer [36] in absorption mode with a zinc selanide ATR probe. The IR data was collected with an average of 32 scans at a spectral resolution of 0.482 cm^{-1} within a spectral range of 4000 – 500 cm^{-1}. Thermo-Galactic [36] software was used for the data collection and further analysis.

4.   Results and Discussion

4.1   Solid-State Synthon Analysis

A detailed analysis of the intermolecular synthons present in the solid state for the α-

and β-forms of PABA has been previously published [6] and the data is summarised in **Figures 6** and **7** and **Table 1**.

Analysis of the higher temperature α-form reveals the strongest synthon (Aα) to be associated with H-bonded carboxylic acid OH…O dimer interactions followed by, in decreasing strength, H2H π-π stacking interactions (Bα), NH…O (Cα) H-bonding interactions and displaced H2H van der Waals interactions (Dα).

In contrast, the strongest intermolecular synthons present within the low temperature β-form involves H2T π-π dimer pair interactions (Aβ), followed by, in deceasing strength, OH…N H-bonding interactions (Bβ), displaced H2T van der Waals interactions (Cβ) and NH…O H-bonding interactions (Dβ).

A noteworthy difference between the two structures lies in the presence of the strong carboxyl acid dimer (Aα) in the α-form which is not present in the β-form structure as well as strong H2T dimer pair interactions (Aβ) and the OH…N H-bonding interactions (Bβ) in the β-form both of which are not present within the α-form structure.
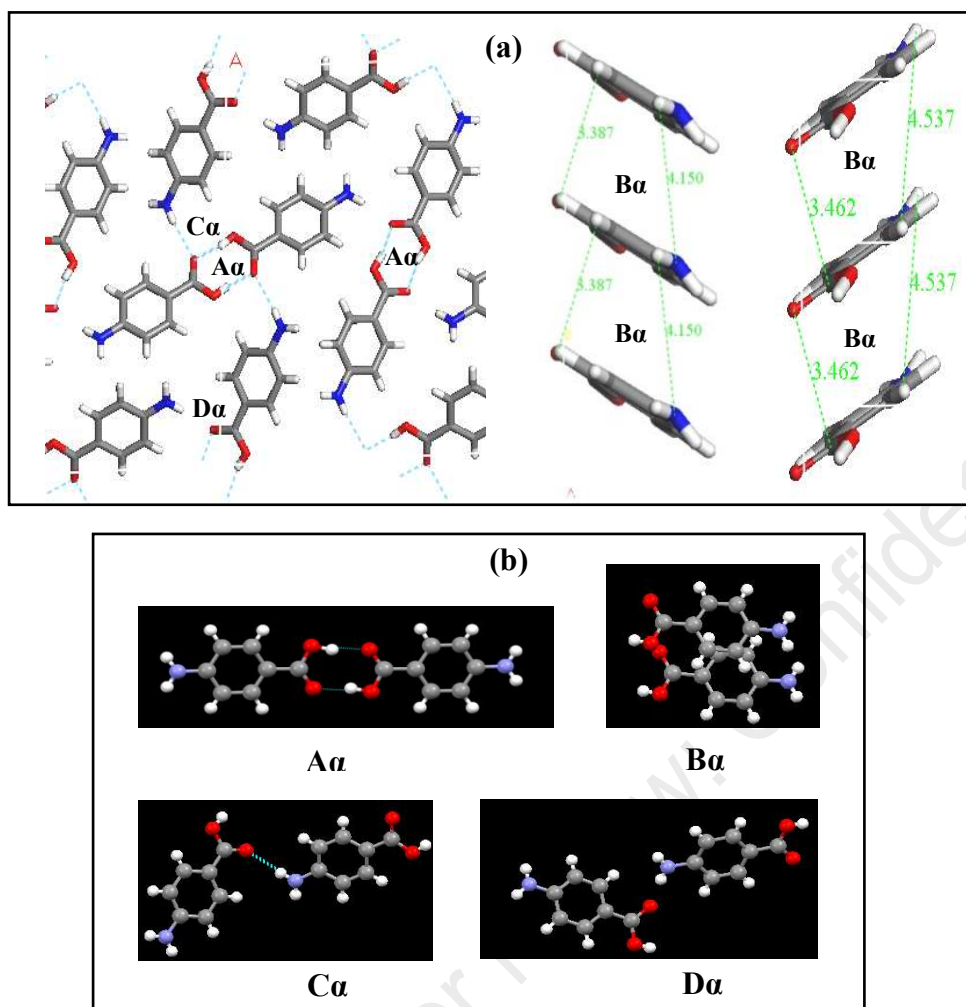
Figure 6. Intermolecular diagrammatic representation of the key synthons present in the α-form of PABA: (a) packing diagrams; (b) molecular pair representation of the synthons highlighting the nature of their interactions (data derived from [6, 25]).
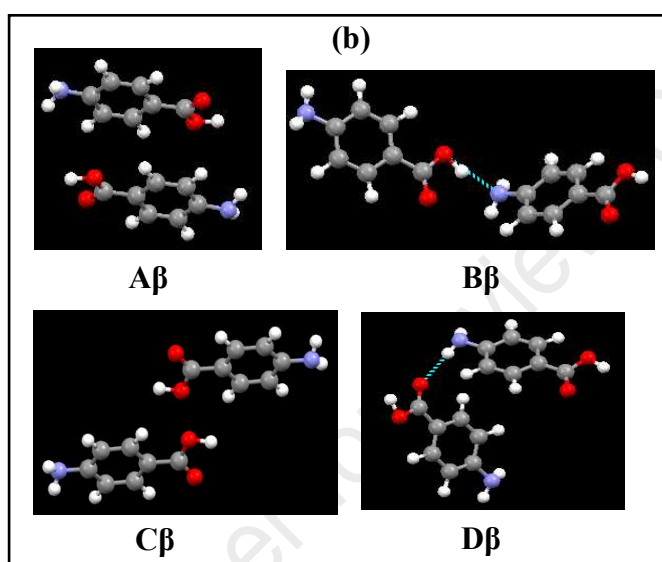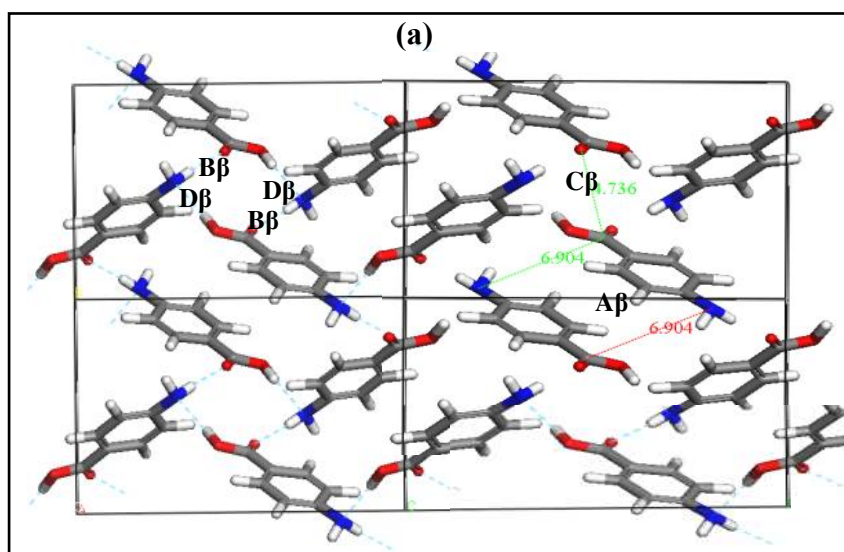
Figure 7. Intermolecular diagrammatic representation of the key synthons present in the β-form of PABA: (a) packing diagrams; (b) molecular pair representation of the synthons highlighting the nature of their interactions (data derived from [6, 25]).

Table 1. Synthon analysis for the α-form (a) and β-form (b) of PABA associated with identification of the strongest intermolecular interactions in the solid state representing ca. 70% of the total lattice energy and highlighting the differing physical chemical nature of the interactions between these two forms (data derived from [6]).

Bond	Multiplicity	Distance (Å)	Intermolecular Energy (kcal/mol)	% Contribution to Lattice Energy	Dominating Interatomic Interaction Type
(a)					
Aα	1	8.23	-5.67	23.1	OH…O H-bonding
Bα	2	3.86	-2.68	21.8	H2H π-π stacking
Cα	1	7.90	-2.27	9.3	NH…O H-bonding
Dα	2	7.96	-2.26	18.4	Displaced H2H vdW
Total			-17.82	72.6	
(b)					
Aβ	1	4.17	-2.57	11.9	H2T π-π dimers
Bβ	2	8.11	-2.45	22.7	OH…N H-bonding
Cβ	2	5.73	-2.39	22.2	Displaced H2T vdW
Dβ	2	6.74	-1.46	13.6	NH…O H-bonding
Total			-15.17	70.4	

4.2 MD Simulations

Since the solubilities of PABA are very different, finding a single concentration that is realistic for an experimental crystallisation experiment was challenging. However, the 0.1 g/ml at 20 °C selected was found to be the closest concentration that was reasonably realistic for all three solvents. In these conditions, the AcN solution was supersaturated, the EtOH solution was saturated and the H_2O solution was extremely supersaturated.

4.2.1 Oxygen – oxygen H-bonding interactions
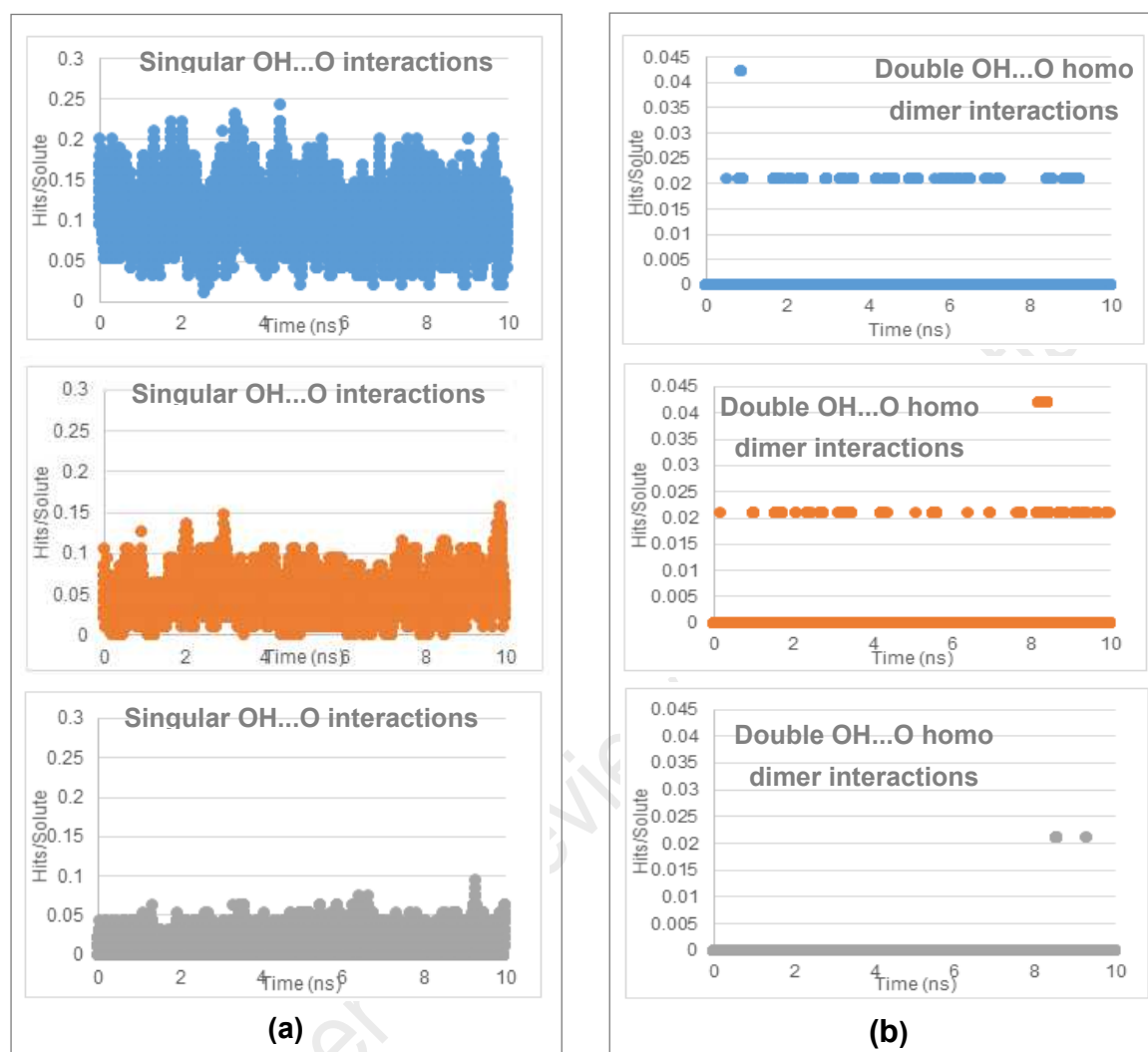
Figure 8. Number of hits found from the searching within MD trajectory files of (a) the singular OH...O interactions and (b) the double OH...O classic homo dimer interactions of PABA in 0.1 g/ml solutions: AcN (blue), EtOH (orange) and H_2O (grey) over a 10 ns simulation. Hits are normalised relative to the amount of solute molecules per simulation.

The propensity for the formation of singular OH…O H-bonding interactions among the carboxylic groups present within the PABA solutions are shown in **Figure 8(a)** revealing that the greatest amount of singular OH…O interactions were found in the AcN solution, followed by the EtOH and then H_2O solutions. It could be argued that as

the solubility of PABA is lower in AcN than EtOH, then it might be expected that there would be a greater degree of solute-solute interactions. However, the solubility of PABA is the lowest in water, where it was found that the OH…O interactions between the solute were also found to be much lower than the same found in AcN and EtOH solutions. It would be, perhaps, more likely that the higher counts found for AcN (H-bond acceptor) reflects its lack of solvation ability with respect to the carboxyl acid group when compared to EtOH (H-bond donor and acceptor). In contrast, the low count for aqueous solution simulation probably reflects the strong solvation ability of water molecules with respect to their strong (only) interactions with the carboxyl acid group.

Examination of the propensities of the OH…O homo dimers (**Figure 8(b)**) associated with synthon Aα were also found in higher amounts in the AcN and EtOH solutions, in comparison to H_2O solutions where they were only observed twice in the 10 ns simulation. It was noteworthy also that these interactions were found in much lower amounts when compared to the singular OH…O interactions and that the propensities were quite similar between AcN and EtOH.

4.2.2 Oxygen – nitrogen H-bonding interactions
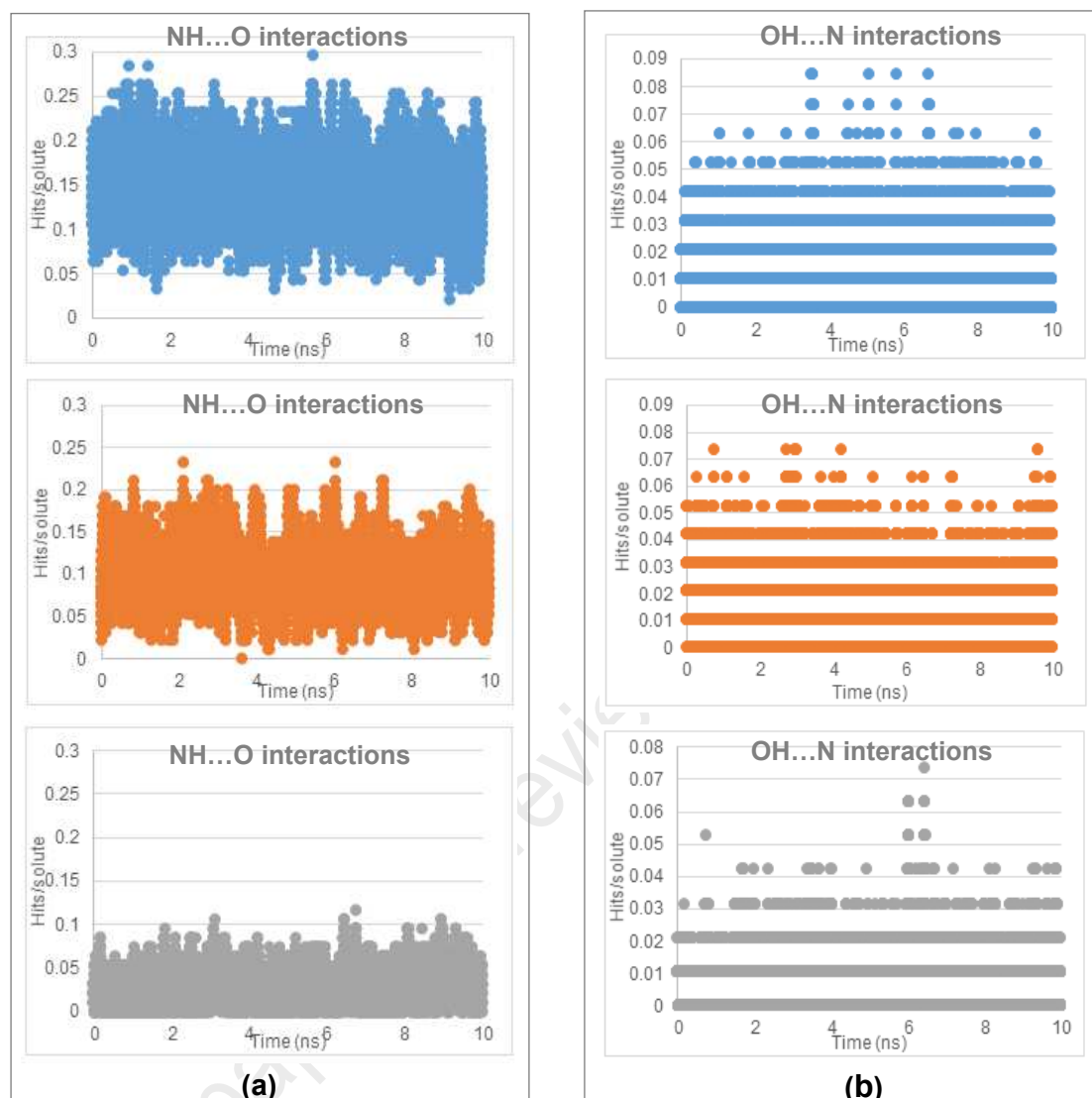
Figure 9. Number of hits found from the searching within MD trajectory files of (a) the singular NH...O interactions and (b) the singular OH...N classic homo dimer interactions of PABA in 0.1 g/ml solutions: AcN (blue), EtOH (orange) and H_2O (grey) over a 10 ns simulation. Hits are normalised relative to the amount of solute molecules per simulation.

Figure 9 highlights the differences in the amounts of NH…O (α- and β-forms) and OH…N (β-form) H-bonding interactions (between amino and carboxylic groups) for the three different solvents with the latter being was found to be lower, when compared

to the NH…O interactions. The NH…O interactions were found to be quite similar between AcN and EtOH but significantly lower in H_2O. The amount of OH…N interactions were found to be quite similar in AcN and EtOH, and, interestingly, only being fractionally lower in H_2O solutions. The OH…N interactions, found only in the β-structure, were found to be lower in all solvents when compared to the NH…O interactions. However, it should also be noted that the amount of NH…O interactions were found to be higher than the OH…O interactions in all three solvents tested.

4.2.3 Strong van der Waals intermolecular bonding interactions
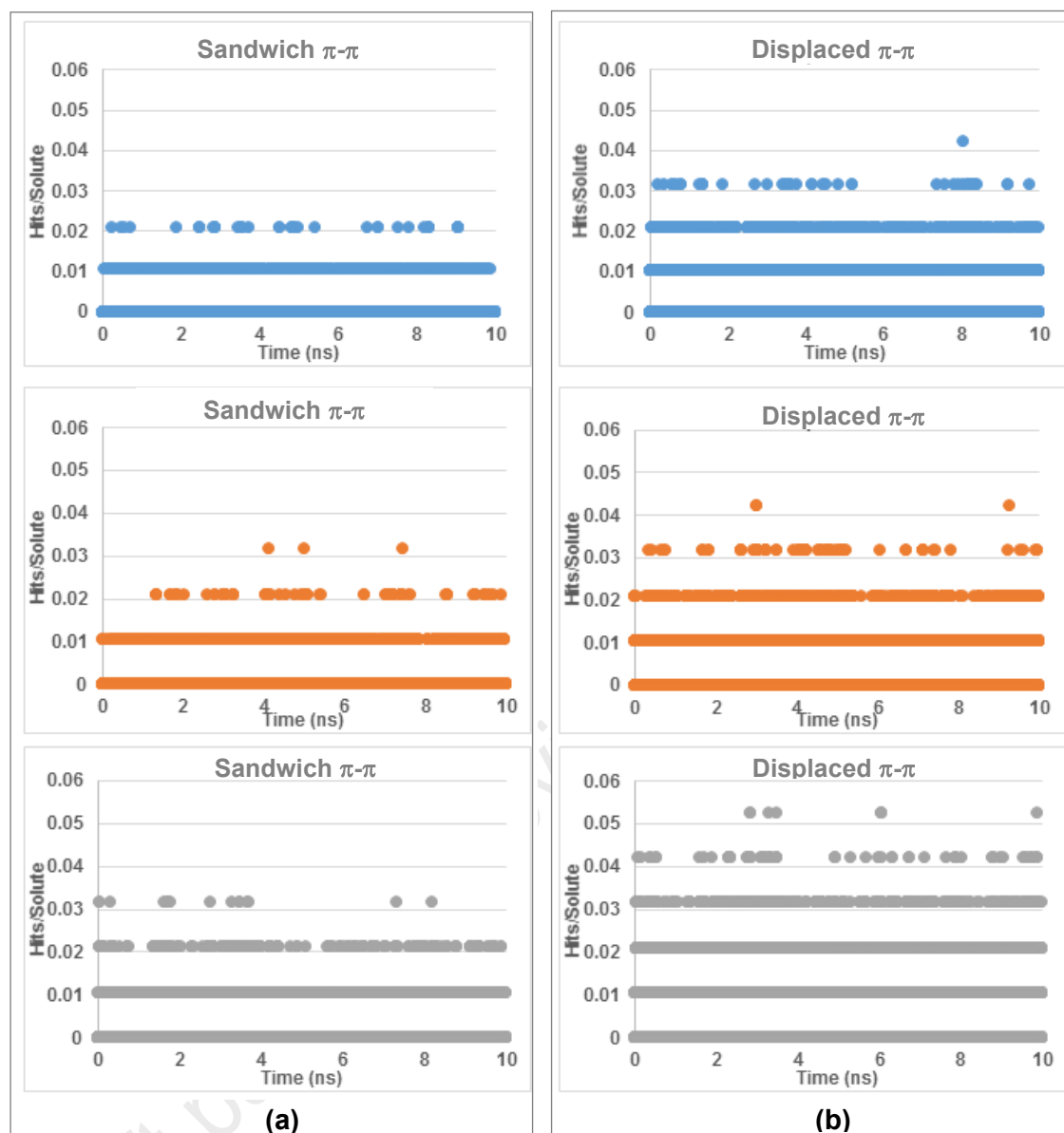
Figure 10. Hits per PABA molecule found from the searching within MD trajectory files of (a) the sandwich $\pi-\pi$ interactions and (b) the displaced $\pi-\pi$ interactions of PABA in 0.1 g/ml solutions: AcN (blue), EtOH (orange) and H_2O (grey) over a 10 ns simulation. Hits are normalised relative to the amount of solute molecules per simulation.

Figure 10 compares the van der Waals interactions between the sandwich (a) and displaced (b) π-π synthons revealing the π displaced interactions to be found in greater numbers when compared to the π sandwich interactions in both the AcN and EtOH

solutions. This is consistent with current knowledge regarding π−π stacking interactions, which reflects that the electrostatic interactions between the negative ring π electrons and the positive ring hydrogens often results in a displaced orientation for the stacking interactions. In contrast to the H-bonding interactions, it is also interesting to note that the sandwich π−π stacking interactions were found to be slightly higher in water than EtOH. Instinctively, one might think that the hydrophobic tail of EtOH would be most likely to disrupt the π−π stacking interactions by forming apolar interactions with the phenyl ring. However, it is likely that the presence of the H-bonding donor proton attracts the EtOH molecules to the more polar COOH and NH_2 groups, resulting in the extra carbon having a negligible effect in decreasing the amount of π−π stacking interactions in the simulation. Overall, the data would be consistent with the hydrophobic aromatic rings tending to close pack in hydrophylic protic solvents such as water and EtOH in comparison with AcN which rends to solvate PABA more equantly in 3D.

The absolute number of hits for each type of interactions throughout each 10 ns simulation is summarised in **Table 2** to provide an improved quantification as to how the different intermolecular interactions change between the different solvents.

Table 2. Absolute number of hits for carboxylic-carboxylic, amino-carboxylic and $\pi-\pi$ stacking interactions found in the three solvents at 0.1 g/ml at 20°C.

Atom-atom Interactions	AcN	EtOH	H$_2$O	Associated Synthons	Comments
Single OH…O	9.99	4.73	0.28	Aα	O both donor & acceptor, only in α-form
Double OH…O	0.068	0.066	0	Aα	O both donor & acceptor, only in α-form
NH…O	13.63	9.30	2.50	Cα, Dβ	N donor & O acceptor, in both forms
OH…N	1.28	1.44	1.12	Bβ	N acceptor, only in β-form
Sandwich π-π	0.0007	0.0010	0.0017	Bα, Aβ	H2H & H2T not differentiated, in both forms
Displaced π-π	0.0027	0.0031	0.0064	Dα, Cβ	H2H & H2T not differentiated, in both forms

Table 2 shows that the absolute number of single OH…O interactions found in EtOH was found to be approximately half those found in AcN. However, in terms of the absolute number of complete dimers found, there was found to be little difference between AcN and EtOH. As was clear in **Figure 8(a)**, the concentration of OH…O interactions found in the aqueous simulations were found to be very low.

4.2.4   Summary

In comparison to the OH…O interactions, the NH…O interactions were found to be only approximately 30% lower in EtOH than AcN, along with these interactions being approximately 80% lower in H$_2$O. This is a significant drop, but much less significant than the drop in OH…O interactions between AcN and H$_2$O, where the OH…O interactions found in H$_2$O were only a fraction of those found in the other solvents. The

data shows only limited differences between the "finger printing" OH…N interactions in all three solvents but importantly the π-π interactions does seem to be favoured in a β-form generating aqueous environment.

4.3   Infrared Spectroscopy Measurements

Solid- and solution-state IR data is given in **Figures 11-13** and in **Table 3**.

4.3.1   Solid-state FTIR spectroscopy

Analysis of the solution state of PABA using IR spectroscopy is severely limited by strong solvent absorption which effectively masks many of the useful spectral features revealed for solution-state structural characterisation. Despite, the carbonyl region is available. **Figure 11** shows the solid-state spectra in the carbonyl region revealing the characteristic absorption bands for the α- and β-forms. These data are also tabulated in **Table 3**.
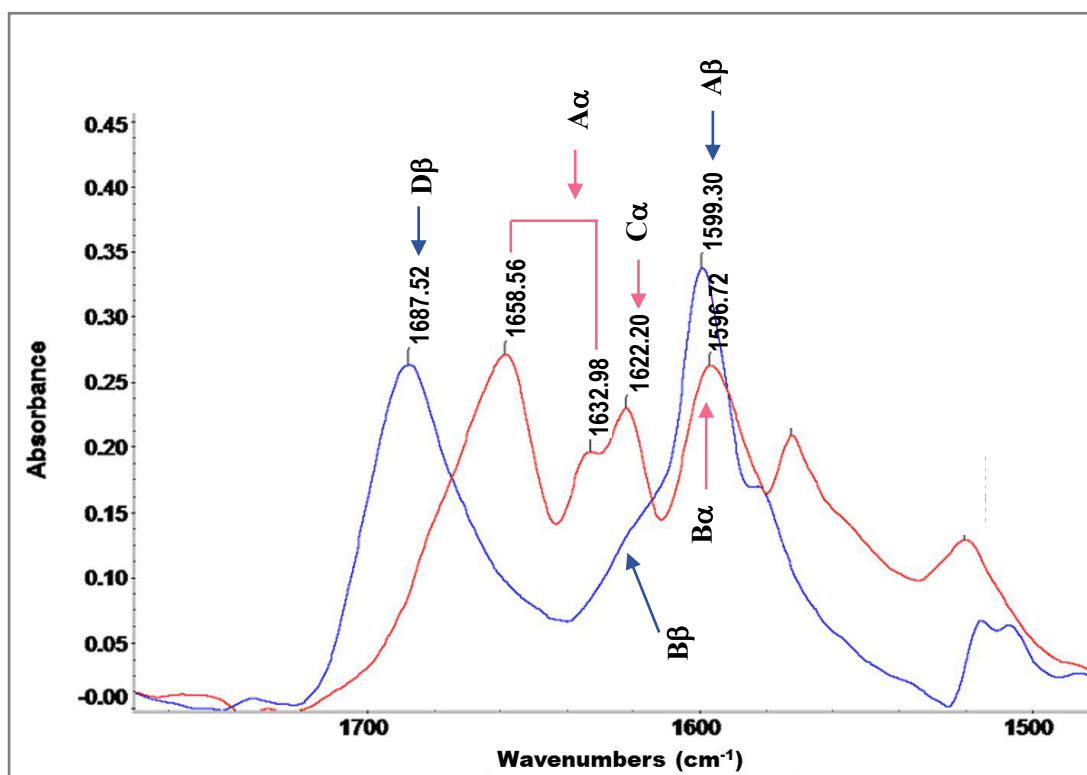
Figure 11. Comparison of the carbonyl region of the α (red) and β (blue) IR spectra (data derived from [26]).

Table 3. List of major the FTIR absorption bands (cm^{-1}) in the solid-state and solution state of PABA close to the carbonyl region. Note that the presence of strong solvent absorption band preclude PABA characterization in the other IR spectral regions (data derived from [26]).

Environment	υ Carbonyl (cm^{-1})			υ Aromatic Ring (cm^{-1})
α-form Solid		1658.56 OH…O (Aα)	1632.98 OH…O (Aα)	1622.20 NH…O (Cα)	1596.72 H2H (Bα)
β-form Solid		1687.52 OH…N (Dβ)		Weak NH…O (Bβ)	1599.30 H2T (Aβ)
EtOH Solution	1710.62 Solvated carboxylate	1684.89 Carboxylate dimer	1640.19 Carboxylate dimer		1606.26
AcN Solution	1710.46 Solvated carboxylate	1678.50 Carboxylate dimer	1633.09 Carboxylate dimer		1605.54

4.3.2 Solution-state FTIR spectroscopy

Figures 12 and **13** show the solution-state spectra recorded as a function of concentration in AcN and EtOH, respectively. For PABA in AcN solvent, the C=O region is well defined with three sharp absorption bands at 1709.99, 1678.24 and 1633.04 cm^{-1}, the two higher wavenumber bands could represent two carbonyl stretching environments due to their proximity to each other, within 40 cm^{-1} which is the expected range for related C=O stretching, monomer and dimer frequencies. This has been observed for a number of systems [37] and can be ascribed to the presence of more effective H-bonding from the solvent which increases the C=O stretching frequency and hence the C=O stretching frequency for a dimerised structure would be expected to lie at a lower wavenumber in comparison. This spectral assignment could thus indicate the presence of a solution-state dimer structure consistent with the analysis of the carbonyl peaks in the solid-state spectra of the α-form. The latter has been seen in a number of carboxylic acid systems including benzoic acid and tetrolic acid [16].
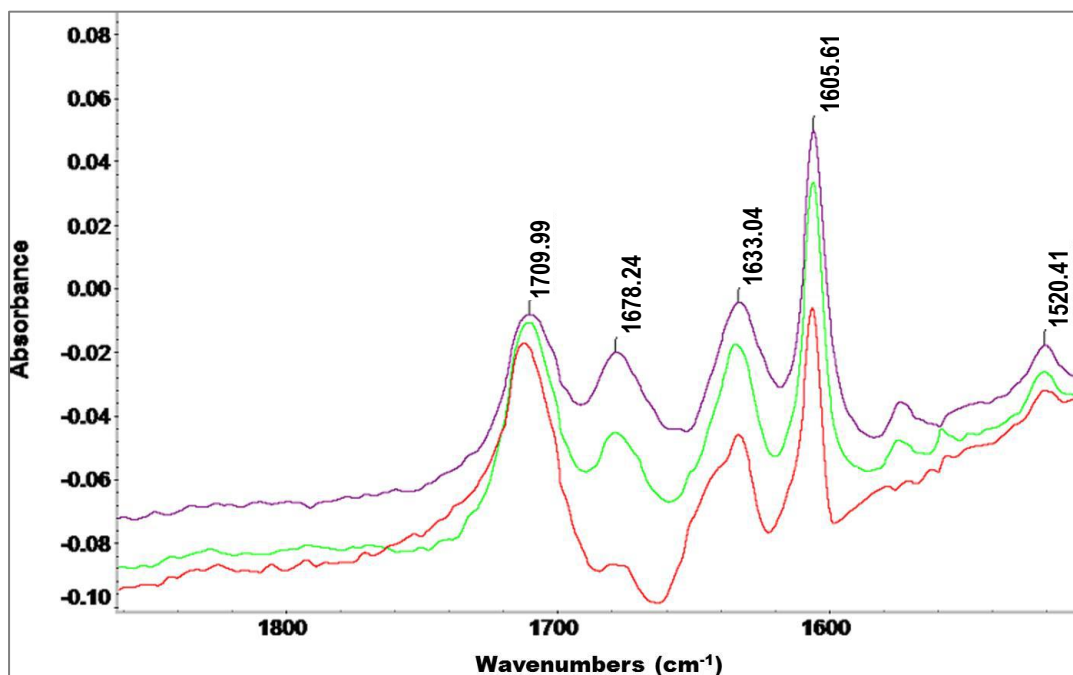
Figure 12. IR spectra of PABA in AcN with three solution concentrations of 64.4 g/kg (purple), 60 g/kg (green) and 55 g/kg (red) at 20 °C, 18 °C and 15 °C (data derived from [26]).

In the dilution experiments for the AcN solution (**Figure 12**), the C=O peak at 1678.24 cm^{-1} can be seen to decrease in intensity with respect to its neighbouring C=O peak at 1709.99 cm^{-1}. This seems to indicate that the peak at 1709.99 cm^{-1} is related to the solvated monomer C=O stretching vibration due to this intensity increase relative to the other C=O frequency as a function of increasing dilution. This will likely be caused by H-bonding between the C=O---H-Me resulted from the induced dipole on the AcN molecule. This dilution effect also seems to suggest that the peak at 1678.24 cm^{-1}, which decreases in intensity upon increase in solvent concentration, is the carbonyl stretching of the carboxylic acid dimer C=O. Upon dilution the two peaks shift in intensity with the peak relating to the solvated monomer intensity increasing and the peak relating to

the carboxylic acid dimer decreasing. This is a good indication that in relatively concentrated solutions of PABA in AcN there is a distribution of solvated monomers and carboxylic acid dimers of PABA.

For the PABA in EtOH solution, **Figure 13** shows that the C=O region is well resolved in EtOH with sharp absorption bands at 1685.72, 1643.13 and 1606.93 cm^{-1}, unlike the AcN carbonyl region these two peaks are not within the expected 40 cm^{-1} wavenumber range and so might not be characterized as being representative of a distribution of monomers and dimers. However on closer inspection of the data, a small shoulder peak is visible on the 1685.72 cm^{-1} carbonyl stretching band, which seems to increase in relative intensity with increasing dilution. Further baseline correction and peak fitting of this data set revealed a peak position at maximum intensity of 1710.62 cm^{-1} of the shoulder peak, which falls within the 40 cm^{-1} of $\Delta \upsilon$ expected for a dimer and monomer population in solution. As such, the data seems to mirror that for AcN solutions, with a major C=O band at ~1685.72 cm^{-1} and a less intense band at 1710.62 cm^{-1} for the two C=O stretches which would relate to the solvated monomer and dimer peaks in the AcN spectra at 1709.99 and 1678.24 cm^{-1}, respectively. This would suggest that in EtOH solutions PABA forms a dimerised molecular structure in saturated and under-saturated solutions as a majority species and which decreases at higher dilution ranges relative to AcN solutions.

36
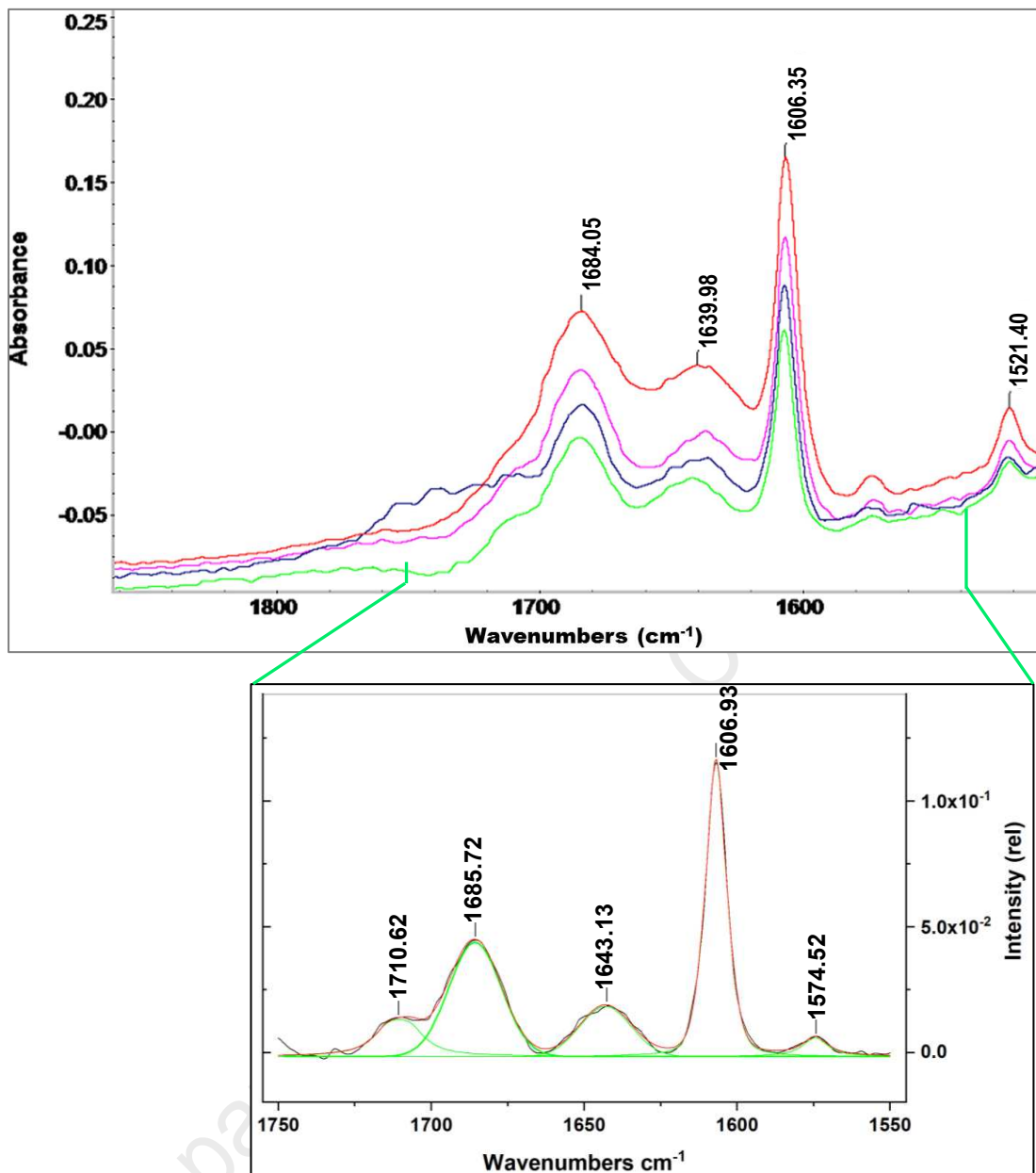
Figure 13. IR spectra of PABA in EtOH with four solution concentrations of 147.7 g/kg (red), 130 g/kg (pink), 110 g/kg (blue) and 80 g/kg (green) at 20 °C, 3 °C, -3 °C and -17 °C. Note that the enlarged spectrum of PABA in EtOH at 80 g/kg was fitted to identify the peak position (1710.62 cm^{-1}) at the shoulder, the highlighted peak positions are fitted peak positions and hence differ from the above (data derived from [26]).

4.3.3 Summary

The solid-state FTIR results provided an understanding of the two key structural

synthons of the centro-symmetric carboxylic acid dimer (**Figure 2(a)**) and the four membered H-bonded ring system (**Figure 2(b)**) found in the crystal structures of α- and β-form PABA, respectively. The dilution experiments in the EtOH and AcN solutions revealed the presence of a distribution of solvated monomers and dimerised PABA molecules in these solutions.

Comparatively, it is noteworthy that the solution-state data show a more reasonable agreement with the IR absorption features which could be expected to template the α-form structure than with those expected to template the β-form structure, notably the strong feature at 1687.5 cm^{-1}.

Overall, the FTIR results of PABA in solid-state and in solutions have demonstrated strong evidence that PABA has the ability to self-associate in saturated solutions. This was confirmed using FTIR spectroscopy in both AcN and EtOH solutions, providing a strong link between the solution-state species present and the primary α-form structural synthon found in the crystal structure. This is a likely cause for the dominant crystallisation of the α-form crystal structure from solution and provides a basis of knowledge for further nucleation studies.

5. Concluding Remarks

A multi-scale modelling approach has linked solid-state synthonic analysis, based upon the crystal structures of PABA, with solution-state characterisation using MD simulations. The latter, facilitated through a detailed description of the solution-state

inter-molecular interactions, has been combined with molecular geometry snapshots taken from the MD trajectory files together with experimental infra-red spectroscopy data. This analysis has yielded intimate details concerning how the functional groups in PABA aggregate within solvation environments, how this is mediated by solvent choice and how this relates to the polymorphic structures that are formed after crystallisation from the solution phase.

Drawing this new data together with a body of previous work sheds new light on the potential molecular pathway that directs solvated molecules within solution to preferentially crystallise in the α rather than β crystallographic form. Specifically, crystallisation of β-form requires greater change in molecular conformation in the solid-state when compared to α-form hence providing a bigger barrier to crystallisation. Crystallisation of β-form also requires the assembly of a larger cluster size to stabilise its structure when compared to α-form consistent with low solution supersaturations being needed to prepare this form. Solid-state characterisation linking to solution-state synthon propensity calculations reveal the α-form's carboxylic acid dimer (synthon Aα) to be a very strong interaction when compared to competing solute/solvent interactions and, thus, one that can be expected to dominate the polymorphism direction process. The exception to this seems to be in aqueous solutions where water, through its strong solvation of the carboxylate group, appears to disrupt the carboxylic acid dimer formation process and hence, at low aqueous supersaturations, the β-form can crystallise, albeit rather slowly. MD calculations were found to be consistent with the

presence of intermolecular interactions between the carboxylic acid (synthon Aα) in solution as well as NH…O H-bonding (synthons Cα, Dβ), π-π (synthons Bα, Aβ) and aromatic displaced ring van der Waals interactions (synthons Dα, Cβ). The MD results are also well-consistent with the experimental crystallisability observation. In particular, OH…O (synthon A) interactions are stronger in AcN when compared to EtOH where the solvation is much stronger. In aqueous solutions, the hydrogen bonded interactions are much lower than for AcN and EtOH. However, in the case of the hydrophobic π-π interactions, their concentrations were found to be higher than for the cases of AcN and EtOH solutions. These is also only rather limited evidence for the presence of other key interactions, notably the β-form's "finger printing" OH… N interactions (synthon Bβ) which is only present in β-form and, at the current stage of analysis, it has not been possible to discriminate between the head-to-head (α-form) and head-to-tail (β-form) aromatic ring interactions.

Whilst the MD studies have provided important information concerning the solution-state structural environment within the solution state, MD simulation times have been far too short to enable the simulations to follow the pathway through to the nucleation event and this aspect is a clear restriction of the approach presented here.

Infra-red spectra in the solution phase (EtOH and AcN solvents) were found to be closely related to the α-form when compared to the β-form structure. The solution IR data was also found to be consistent with the presence of both solvated monomers and carboxylic acid dimers (synthon Aα) in solution, albeit strong solvent absorption

precluded IR characterisation within aqueous solutions. The MD synthon propensity and PABA solvation studies all support this model notably through examining the relative populations of π-π dimer pair interactions (synthon Aβ) versus OH…O H-bonding dimers (synthon Aα) which suggests the latter templates the greater crystallisability of PABA in AcN with respect to EtOH associated with the latter's higher solvation energy.

In terms of how the crystallisation and polymorph selection process is mediated by solvent selection, van't Hoff analysis reveals less than ideal solubility, low solvation energy and, hence, favourable solute-solute interactions in the order of water > AcN > EtOH. This behaviour is matched by wider meta-stable zone widths and lower nucleation rates, respectively, encompassed within an instantaneous nucleation mechanism (except at low solute concentrations) which are consistent with the formation of solute pre-nucleation clusters in solution.

The above model is also supported through SAXS measurements in ethanolic solutions which illustrate the progress from poorly ordered pre-nucleation clusters in undersaturated solutions through to their development and the accompanying transformation of PABA molecular entities from monomers to dimers during crystallisation process. These studies are, though quite limited in extent as solute contrasting issues precluded wider applications as a function of both solvent type and solute concentration notably in cases where the transformation between progressive to instantaneous nucleation mechanism at low solute concentrations could be probed. A

further open question centres whether the subsequent nucleation process progresses within the evolving solute clusters through an annealing recrystallisation mechanism of the solute clusters or at the interface between the supersaturated solution and the cluster surfaces, for example by a secondary nucleation/templating mechanism. Further studies are clearly needed to elucidate this aspect.

Overall, this study further demonstrates the attractive potential for this comparatively user-friendly crystallographically-based multiscale modelling approach which integrates solid-state and MD simulations. Its strengths highlight the ease of input file construction, MD simulations and synthon analysis of the trajectories of organic molecular solutions. The synergy of these calculations with related high-level electronic structure DFT calculations of synthon polarizability and propensity has provided a further degree of granulation and quantification to the fine details of the solution chemistry. The study's further integration with a wide range of experimental data highlights the added-value of combining multi-scale modelling with multi-technique crystallisation characterization using in-process analysis techniques. It also demonstrates the inherent strengths in exploring the molecular-scale transition pathway from solution through aggregation/nucleation to the direction of the polymorphic form of the resultant crystals which would be inaccessible from a single modelling or experimental technique.

Acknowledgements

42

paper. Research into characterising the structural pathway associated with the nucleation of the PABA system was initiated through an EPSRC Critical Mass programme (Molecules, Clusters and Crystals: Grants EP/I014446/1 and EP/I013563/1) in collaboration with the University of Manchester which involved the PhD programmes of two of the co-authors (IR [19] and TDT [26]). This work also builds upon software developments funded through the Synthonic Engineering Program supported by the EPSRC (Grant EP/I028293/1) in collaboration with Pfizer, Boeringer-Ingellheim, Novartis, and Syngenta. The MD modelling research presented here was supported through the Advanced Manufacturing Supply Chain Initiative associated with the 'Advanced Digital Design of Pharmaceutical Therapeutics' (Grant No. 14060) project. In the latter respect, some of the development of the DL_ANALYSER software was supported under the auspices of the EPSRC's Collaborative Computational Project No. 5 (CCP5) (Grant: EP/M022617/1).

Disclosure Statement

No potential conflict of interest was reported by the authors.

References

1.   Faraday Discussions, *Faraday Discussions*, 2015, **177**, 1-560 (ISSN: 1359-6640 (print); 1364-5498 (web)).
2.   R. B. Hammond, K. Pencheva and K. J. Roberts, *CrystEngComm*, 2012, **14**, 1069-1082.
3.   C. Wang, I. Rosbottom, T. D. Turner, S. Laing, A. Maloney, A. Y. Sheikh, R. Docherty, Y. Q. and K. J. Roberts, *Pharmaceutical Research*, 2021, **38**, 971-990.
4.   T. D. Turner, X. X Lai and K. J. Roberts, *CrystEngComm*, 2018, **20**, 4099–4102.
5.   A. A. Moldovan, I. Rosbottom, V. Ramachandran, C. M. Pask, O. Olomukhoro and K. J. Roberts, *J. Pharm. Sci.*, 2017, **106**, 882-891.
6.   I. Rosbottom, K. J. Roberts and R. Docherty, *CrystEngComm*, 2015, **17**, 5768-5788.

7. N. Anuar, W. R. Wan Daud, K. J. Roberts, S. K. Kamarudin and S. M. Tasirin, *Crystal Growth & Design*, 2012, **12**, 2195-2203.

8. T. D. Turner, L. E. Hatcher, C. C. Wilson and K. J. Roberts, *J. Pharm. Sci.*, 2019, **108**, 1637-1922.

9. I. Rosbottom, J. H. Pickering, B. Etbon, R. B. Hammond and K. J. Roberts, *Physical Chemistry Chemical Physics*, 2018, **20**, 11622-11633.

10. T. T. H. Nguyen, R. B. Hammond, I. D. Styliari, D. Murnane and K. J. Roberts, *CrystEngComm*, 2020, **22**, 3347-3360.

11. V. Ramachandran, D. Murnane, R. B. Hammond, J. H. Pickering, K. J. Roberts, M. Soufian, B. Forbes, S. Jaffari, G. P. Martin, E. Collins and K. Pencheva, *Molecular Pharmaceutics*, 2015, 18-33.

12. T. D. Turner, P. Gajjar, I. Fragkopoulos, J. Carr, T. T. H. Nguyen, D. Hooper, F. Clarke, N. Dawson, P. Withers and K. J. Roberts, *Crystal Growth & Design*, 2020, **20**, 4252–4263.

13. C. W. Yong, *Journal of Chemical Information and Modeling*, 2016, **56**, 1405-1409.

14. C. W. Yong and I. T. Todorov, *Molecules*, 2018, **23**, article no. 36.

15. I. Rosbottom, C. W. Yong, D. L. Geatches, R. B. Hammond, I. T. Todorov and K. J. Roberts, *Molecular Simulation*, 2021, **47**, 257-272.

16. R. J. Davey, G. Dent, R. K. Mughal and S. Parveen, *Crystal Growth & Design*, 2006, **6**, 1788-1796.

17. M. Svard, F. L. Nordström, E.-M. Hoffmann, B. Aziz and A. C. Rasmuson, *CrystEngComm*, 2013, **15**, 5020-5031.

18. M. J. Bryant, S. N. Black, H. Blade, R. Docherty, A. G. P. Maloney and S. C. Taylor, *J. Pharm. Sci.*, 2019, **108**, 1655-1662.

19. I. Rosbottom, PhD, PhD Thesis, University of Leeds, UK, 2015.

20. I. Rosbottom, D. Toroz, R. B. Hammond and K. J. Roberts, *CrystEngComm*, 2018, **20**, 7543-7555.

21. R. B. Hammond, C. Y. Ma, K. J. Roberts, P. Y. Ghi and R. K. Harris, *The Journal of Physical Chemistry B*, 2003, **107**, 11820-11826.

22. R. B. Hammond, R. S. R S Hashim, C. Y. Ma and K. J. Roberts, *J. Pharm. Sci.*, 2006, **95**, 2361-2372.

23. I. Rosbottom, J. H. Pickering, R. B. Hammond and K. J. Roberts, *Organic Process Research & Development*, 2020, **24**, 500−507.

24. T. D. Turner, D. M. C. Corzo, D. Toroz, A. Curtis, M. M. Dos Santos, R. B. Hammond, X. Lai and K. J. Roberts, *Physical Chemistry Chemical Physics*, 2016, **18**, 27507-27520.

25. D. Toroz, I. Rosbottom, T. D. Turner, D. M. C. Corzo, R. B. Hammond, X. Lai and K. J. Roberts, *Faraday Discussions*, 2015, **179**, 79-114.

26. T. D. Turner, PhD, PhD Thesis, University of Leeds, UK, 2015.

27. A. S. Myerson and P. Y. Lo, *Journal of Crystal Growth*, 1990, **99**, 1048-1052.

28. H. C. Groen and K. J. Roberts, *Journal of Physical Chemistry B*, 2001, **105**, 10723-10730.

29. N. Salwani Md Azmi, N. Anuar, N. Fitrah Abu Bakar, N. Fadhilah Kamalul Aripin and K. J. Roberts, *Journal of Crystal Growth*, 2019, **519**, 91-99.

30. I. T. Todorov, W. Smith, K. Trachenko and M. T. Dove, *Journal of Materials Chemistry*, 2006, **16**, 1911-1918.

31. DL_Software is the collective term for a range of scientific software developed at the Daresbury Laboratory, spanning across multi-length and -time scales. https://www.scd.stfc.ac.uk/Pages/Materials-Modelling-Software.aspx.

32. W. D. Cornell, P. Cieplak, C. I. Bayly, I. R. Gould, K. M. Merz, D. M. Ferguson, D. C. Spellmeyer, T. Fox, J. W. Caldwell and P. A. Kollman, *Journal of the American Chemical Society*, 1995, **117**, 5179-5197.

33. R. A. Sullivan, R. J. Davey, G. Sadiq, G. Dent, K. R. Back, J. H. Ter Horst, D. Toroz and R. B. Hammond, *Crystal Growth & Design*, 2014, **14**, 2689-2696.

34. H. J. C. Berendsen, J. P. M. Postma, W. F. V. Gunsteren, A. DiNola and J. R. Haak, *Journal of Physical Chemistry*, 1984, **81**, 3684-3690.

35. W. G. Hoover, *Physical Review A*, 1985, **31**, 1695-1697.

36. Thermo, *Journal*, 2015.

37. P. Novak, D. Vikić-Topić, Z. Meić, S. Sekušak and A. Sabljić, *Journal of Molecular Structure*, 1995, **356**, 131-141.